A Green Function-Based Parasitic Extraction Method for Inhomogeneous Substrate Layers

Chenggang Xu, Ranjit Gharpurey[+], Terri S. Fiez, and Kartikeya Mayaram

School of EECS, Oregon State University, Corvallis, OR 97331
[+]Dept. of EECS, University of Michigan, Ann Arbor, MI 48109

{cgxu, terri, karti}@ece.orst.edu, [+]ranjitg@eecs.umich.edu

ABSTRACT

This paper presents a new Green function-based approach for substrate parasitic extraction in substrates with inhomogeneous layers. This new formulation allows analysis of noise coupling with sinkers, trenches and wells, - a limitation in prior Green function-based extractors. Numerical examples for sinkers and trenches are provided and compared with the results from three-dimensional semiconductor device simulations. It is shown that the proposed method is accurate and computationally efficient.

Categories and Subject Descriptors

B7.2 [Integrated Circuits]: Design Aids - Simulation, Verification.

General Terms

Algorithms.

Keywords

Substrate noise, parasitic extraction, Green function.

1. INTRODUCTION

With the continuous increase in chip complexity, device density and circuit speed, substrate noise has become one of the major concerns in ICs [1-13]. Different methods have been proposed and applied to the extraction of parasitics. Depending on whether the meshing is over the substrate body or just its boundaries, all these methods can be generally divided into two categories, the volume element methods, i.e., the finite difference method (FDM) or the finite element method (FEM) [5-9] and the boundary element methods (BEM) [10-13]. Fine mesh requirements make the volume methods slow for large-scale problems. The boundary element methods, on the other hand, result in a much smaller matrix size and show much better computational efficiency when discrete sine or cosine transforms are used [10-12]. However, the Green function techniques are typically limited to a substrate that can be approximated as a multilayer structure, and each of these layers has a uniform conductivity and/or permittivity [10]. This limits the application of these methods to modern day processes where substrates may have sinkers, trenches and wells, as shown in Fig. 1 for a BiCMOS process. Clearly the homogeneous layered approximation can not be used for this process.

One way to deal with the lateral variation in the material property is to use a combined boundary element and finite difference method (BEM/FDM), or a combined boundary element and finite element method (BEM/FEM) [14, 15]. In these approaches, a substrate is divided into two parts, as shown in Fig. 2, the top part consists of the inhomogeneous material, and finite element or finite difference methods are used for this region. The bottom part is layer-wise homogeneous, and the boundary element method is used. The two regions are connected such that a boundary element panel is associated with a finite element or finite difference node on the interface. This method needs FEM/FDM meshing for the whole volume of the top inhomogeneous region, and BEM meshing for the interface. Compared to the full FEM or FDM, this method uses volume-meshing for part of the substrate volume, and thus saves memory and improves the computational efficiency. On the other hand, when compared with the full BEM, this method needs to mesh the interface of two large regions, instead of meshing only the contacts. Thus more panels are created, which requires larger computational resources. However, the combined BEM/FEM or BEM/FDM approaches improve FEM or FDM's computational efficiency by sacrificing some of the computational efficiency of the BEM.
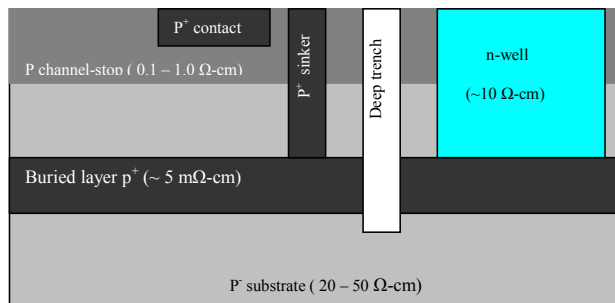

Fig. 1: Cross section of a BiCMOS process with approximate resistivities.
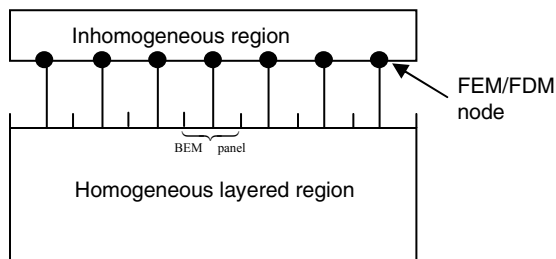

Fig. 2: Schematic for the combined BEM/FEM or BEM/FDM method.

The combined BEM/FEM and BEM/FDM in [14, 15] can be further improved by a so called 'two-problem' approach. The basic idea of this approach was proposed in [8]. To the authors' best knowledge, this method has not been used in practice. This method is based on the observation that, lateral inhomogeneity is caused by local variations such as trenches, sinkers and wells, with the rest of the substrate being laterally homogeneous. We will call these local feature regions 'L-regions', and the surfaces of the L-regions the 'L-surfaces'. With the two-problem approach, a substrate does not need to be split into two distinct regions. The volume meshing is only needed for the L-regions, and the BEM meshing is only needed for the L-surfaces, which is much smaller than the interface in the combined BEM/FEM and BEM/FDM in [14, 15].

This paper develops the two-problem approach and applies it for extracting parasitics in substrates with lateral variations. The organization is as follows: Section II provides to a brief outline of the previous Green function based methods in [11] for laterally homogeneous substrates. Section III details the 'two-problem' approach and the related equation derivation. Examples are presented in Section IV including comparisons with three-dimension device simulations. Conclusions are provided in Section V.

2. GREEN FUNCTION METHOD FORHOMOGENEOUS LAYERED SUBSTRATES

Although the conductance extraction and capacitance extraction are physically different, they are mathematically similar [10, 11]. For convenience of referring to the previous work in [10] and [11], we outline the method based on capacitance extraction.
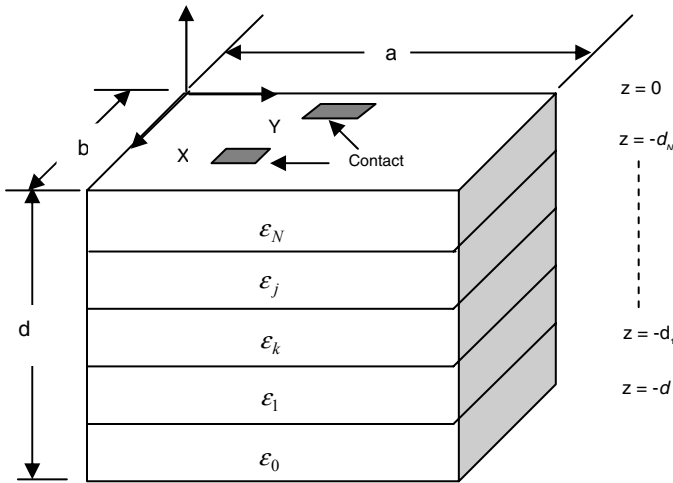

Fig.3: Substrate as a multilayer structure.

Physically, a Green function $G(x_f, y_f, z_f, x_s, y_s, z_s)$ represents the potential at a field point at (x_f, y_f, z_f) induced by a point charge source at (x_s, y_s, z_s) under specified boundary conditions. Once the Green function is given, the matrix of potential, $[P]$, can be calculated, which relates contact potential, $\{V\}$, to their charges, $\{Q\}$, in such a way that

$$[P]\{Q\} = \{V\} \tag{1}$$

and any entry of the matrix $[P]$ can be expressed as

$$p_{\xi\eta} = \frac{\iint\limits_{V_\xi V_\eta} G(x_f, y_f, z_f, x_s, y_s, z_s) dx_s dy_s dz_s dx_f dy_f dz_f}{V_\xi V_\eta} \tag{2}$$

where V_ξ and V_η are the volumes of contact ξ and contact η, respectively. Once the matrix of potential is established the capacitances can then be calculated.

For a homogeneous layered substrate, as shown in Fig. 3, the Green function can be expressed as a double infinite summation. For a field (or observation) point in the j-th layer and a source point in the k-th layer the Green function can be expressed as [11]

$$G_{jk}^{u,l} = G_{jk,0}^{u,l} +$$

$$\sum_{\substack{m=0 \\ m+n\neq0}}^{\infty} \sum_{n=0}^{\infty} \frac{c_{mn}\varphi_{jk}^{u,l}}{ab\varepsilon_k\gamma_{mn}} \cos\frac{m\pi x_f}{a} \cos\frac{n\pi y_f}{b} \cos\frac{m\pi x_s}{a} \cos\frac{n\pi y_s}{b} \tag{3}$$

where, the superscripts u and l indicate the upper and lower solutions, depending on whether the field point (or observation point) is above or below the source point. a and b are the substrate dimension in the x- and y- directions, respectively, as shown in Fig. 3. More details about this equation can be found in [11].

3. THE TWO-PROBLEM APPROACH FOR INHOMEGENEOUS LAYERS

In this section, details of the two-problem approach are presented. For simplicity, but without loss of generality, we assume as shown in Fig. 4, there are two contacts ξ and η on the top of a substrate and the permittivity of the substrate layer is ε_N. There is a L-region with a permittivity of ε^* ($\varepsilon^* \neq \varepsilon_N$) in the substrate. We are interested in the coupling parasitics between these two contacts.
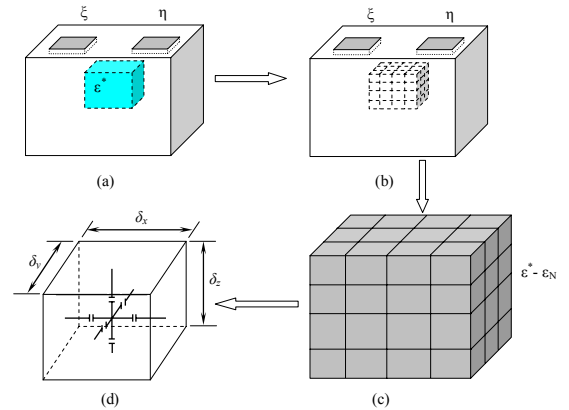

Fig. 4: Schematic for the two-problem approach for lateral permittivity variation. (a) The original problem. (b) Virtual contacts around a L-region. (c) Discretization of the C-region and (d) parasitic network for a cubic cell inside the C-region.

The first step in the two-problem approach is to remove the L-region and fill the cavity with the substrate material to make it laterally homogeneous. The previous interface, i.e., the L-surface,

is assumed to be still there. The L-surface is then meshed into panels. We call these panels virtual contacts. The first problem takes the virtual contacts to be the same as real contacts, and extracts the corresponding parasitic network. Since the substrate is now layer-wise homogeneous, the Green function derived in [11] can be used.

It needs to be noted that, real contacts, such as contacts ξ and η are three-dimensional. However, since the contact thickness is usually much smaller than its lateral dimensions, contacts can be approximated as planar contacts in the x-y plane with zero thickness [10-12]. In the first problem in the two-problem approach, all the virtual contacts are planar contacts with zero thickness. As shown in Fig. 4 (b), these planar contacts can be horizontal or vertical. Equations to calculate the entries of $[P]$ matrix in Eq. (1) related to horizontal zero-thickness contacts can be found in [11]. The equations related to vertical zero-thickness contacts can be derived from the equations for general three-dimensional contacts. A vertical two-dimensional contact is taken as a special case of a three-dimensional contact with its x- or y-dimension shrunk to zero.
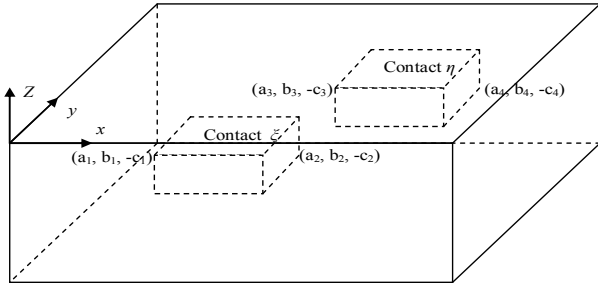

Fig.5: Definition of three-dimensional contacts.

For the contact coordinates shown in Fig. 5, substituting Eq. (3) into Eq. (2) gives,

$$p_{\xi\eta} = G_{jk,0}^{l,u} + p_{\xi\eta}^{**} + p_{\xi\eta}^{*0} + p_{\xi\eta}^{0*} \tag{4}$$

where $G_{jk,0}^{l,u}$ is a constant depending on the substrate thickness and resistivity, and

$$p_{\xi\eta}^{**} = \frac{a^2 b^2}{\pi^4} \sum_{m=1}^{\infty} \sum_{n=1}^{\infty} \frac{4 f_{\xi\eta}}{m^2 n^2} \times$$
$$\frac{\sin\left(m\pi \frac{a_2}{a}\right) - \sin\left(m\pi \frac{a_1}{a}\right)}{a_2 - a_1} \times \frac{\sin\left(m\pi \frac{a_4}{a}\right) - \sin\left(m\pi \frac{a_3}{a}\right)}{a_4 - a_3} \times$$
$$\frac{\sin\left(n\pi \frac{b_2}{b}\right) - \sin\left(n\pi \frac{b_1}{b}\right)}{b_2 - b_1} \times \frac{\sin\left(n\pi \frac{b_4}{b}\right) - \sin\left(n\pi \frac{b_3}{b}\right)}{b_4 - b_3}$$

$$\tag{5}$$

$$p_{\xi\eta}^{*0} = \frac{a^2}{\pi^2} \sum_{m=1}^{\infty} \frac{2 f_{\xi\eta}}{m^2} \times$$
$$\frac{\sin\left(m\pi \frac{a_2}{a}\right) - \sin\left(m\pi \frac{a_1}{a}\right)}{a_2 - a_1} \times \frac{\sin\left(m\pi \frac{a_4}{a}\right) - \sin\left(m\pi \frac{a_3}{a}\right)}{a_4 - a_3}$$

$$\tag{6}$$

$$p_{\xi\eta}^{0*} = \frac{b^2}{\pi^2} \sum_{n=1}^{\infty} \frac{2 f_{\xi\eta}}{n^2} \times$$
$$\frac{\sin\left(n\pi \frac{b_2}{b}\right) - \sin\left(n\pi \frac{b_1}{b}\right)}{b_2 - b_1} \times \frac{\sin\left(n\pi \frac{b_4}{b}\right) - \sin\left(n\pi \frac{b_3}{b}\right)}{b_4 - b_3} \tag{7}$$

$$f_{\xi\eta} = \frac{1}{(c_2 - c_1)(c_4 - c_3)} \left[\int_{-c_2}^{-c_1} \int_{-c_4}^{-c_3} \varphi^{u,l} dz_f dz_s \right] \tag{8}$$

As an example of the equation derivation for vertical planar contacts, we shrink the x-dimension of contact ξ to zero to derive the equations for calculating the coupling between a planar contact in the y-z plane and a three-dimensional contact. Equations for other cases can be derived in a similar manner.

It can be shown that

$$\lim_{|a_j - a_i| \to 0} \frac{\sin\left(m\pi \frac{a_j}{a}\right) - \sin\left(m\pi \frac{a_i}{a}\right)}{a_j - a_i} = \cos\left(m\pi \frac{a_i}{a}\right) \frac{m\pi}{a} \tag{9}$$

By the use of Eq. (9), Eq. (5) can be expressed as

$$p_{\xi\eta}^{**} = \frac{ab^2}{\pi^3} \frac{\sum_{m=1}^{\infty} \sum_{n=1}^{\infty} \frac{f_{\xi\eta}}{mn^2}}{(a_4 - a_3)(b_2 - b_1)(b_4 - b_3)} \times$$
$$\left(\begin{array}{l} -\sin\left(m\pi \frac{a_2 - a_4}{a}\right) + \sin\left(m\pi \frac{a_4 + a_2}{a}\right) + \\ \sin\left(m\pi \frac{a_2 - a_3}{a}\right) - \sin\left(m\pi \frac{a_3 + a_2}{a}\right) \end{array} \right) \times$$
$$\left[\begin{array}{l} \cos\left(n\pi \frac{b_2 - b_4}{b}\right) - \cos\left(n\pi \frac{b_2 + b_4}{b}\right) - \cos\left(n\pi \frac{b_2 - b_3}{b}\right) + \\ \cos\left(n\pi \frac{b_2 + b_3}{b}\right) - \cos\left(n\pi \frac{b_1 - b_4}{b}\right) + \cos\left(n\pi \frac{b_1 + b_4}{b}\right) + \\ \cos\left(n\pi \frac{b_1 - b_3}{b}\right) - \cos\left(n\pi \frac{b_1 + b_3}{b}\right) \end{array} \right]$$

$$\tag{10}$$

Similarly, for $p_{\xi\eta}^{*0}$, we have

$$p_{\xi\eta}^{*0} = \frac{a}{\pi(a_4 - a_3)} \sum_{m=1}^{\infty} \frac{f_{\xi\eta}}{m} \times$$
$$\left(\begin{array}{l} -\sin\left(m\pi \frac{a_2 - a_4}{a}\right) + \sin\left(m\pi \frac{a_4 + a_2}{a}\right) + \\ \sin\left(m\pi \frac{a_2 - a_3}{a}\right) - \sin\left(m\pi \frac{a_3 + a_2}{a}\right) \end{array} \right)$$

$$\tag{11}$$

Eq. (7) for $p_{\xi\eta}^{0*}$ does not change with the shrinking of the x-dimension.

Expanding Eq. (10) results in 32 terms of mixed discrete sine-cosine transforms (MDSCT) in the following form

$$\sum_{m=0}^{M-1}\sum_{n=0}^{N-1} F_{mn} \sin\left(m\pi\frac{p}{M}\right)\cos\left(n\pi\frac{q}{N}\right) \qquad (12)$$

Eq. (12) can be calculated efficiently in a similar way as the two-dimensional DCT or DST. It needs (M-1) one-dimensional DCTs, followed by (N-1) one-dimensional DSTs [16]. Eq. (11) can be calculated by four one-dimensional DSTs. Expanding Eq. (7) results in eight one-dimensional DCTs.

The second problem is a grid representation of the internal parasitic network of a region with a permittivity equal to $\varepsilon^*- \varepsilon_N$, and an outer surface a 'copy' of that of the L-region. We call this region a companion region, or a C-region. When the C-region is meshed into cubes, as shown in Fig. 4 (c), each of these cubes has an internal parasitic network, as shown in Fig. 4 (d). The parasitics in the x-, y- and z-directions can be calculated by

$$C_x = 2\frac{\varepsilon\delta_y\delta_z}{\delta_x}, \quad C_y = 2\frac{\varepsilon\delta_x\delta_z}{\delta_y}, \quad C_z = 2\frac{\varepsilon\delta_y\delta_x}{\delta_z} \qquad (13)$$

where $\varepsilon = \varepsilon^* - \varepsilon_N$ is the permittivity of the C-region.

The solution to the original problem can be obtained by putting the parasitic network for the C-region in parallel with the parasitic network from the first problem. The resultant network can then be included in a circuit simulator to compute the effect of the lateral variation, as suggested in [10]. However, this would significantly increase the number of nodes in simulation, and, therefore, is not computationally efficient. A better way is to lump the parasitic network to the original contacts. This can be done in the following manner [9]:

Let the matrix of capacitances for the resultant capacitance network be $[C_T]$, which relates the node voltage, $\{V_T\}$, to the charges, $\{Q_T\}$,

$$[C_T]\{V_T\} = \{Q_T\} \qquad (14)$$

Let the total number of real contacts be N. Now we are looking for a model, $[C_C]_{N\times N}$, that relates the voltages at these real contacts, $\{V_C\}_N$ to their charges, $\{Q_C\}_N$, by

$$[C_C]\{V_C\} = \{Q_C\} \qquad (15)$$

Clearly, $\{V_C\}_N$ and $\{Q_C\}_N$ are the subsets of $\{V_T\}$ and $\{Q_T\}$, respectively. We can, therefore, write

$$\{V_T\} = \begin{Bmatrix} V_C \\ V_I \end{Bmatrix}, \quad \{Q_T\} = \begin{Bmatrix} Q_C \\ Q_I \end{Bmatrix} \qquad (16)$$

where $\{V_I\}$ and $\{Q_I\}$ are the voltages and charge related to nodes that are not connected to the real contacts.

By using Eq. (16), Eq. (15) can be recast as

$$\begin{bmatrix} C_{CC} & C_{CI} \\ C_{IC} & C_{II} \end{bmatrix}\begin{Bmatrix} V_C \\ V_I \end{Bmatrix} = \begin{Bmatrix} Q_C \\ Q_I \end{Bmatrix} \qquad (17)$$

Since only the real contact nodes can have a non-zero charge, i.e. $\{Q_I\} = 0$,

$$\{Q_C\} = \left[C_{CC} - C_{CI}C_{II}^{-1}C_{IC}\right]\{V_C\} \qquad (18)$$

Thus

$$[C_C] = \left[C_{CC} - C_{CI}C_{II}^{-1}C_{IC}\right] \qquad (19)$$

4. NUMERICAL EXAMPLES

The two-problem method has been implemented in a solver called EPIC (Extraction of Parasitics in ICs). In this section, simulation examples with EPIC are presented, and comparisons with the results from ATLAS [17], a commercial semiconductor device solver, are also provided.

We consider two identical square contacts of size 10μm×10μm that are separated by a L-region, as shown in Fig. 6 (a), (b). The corresponding π-resistance network is shown in Fig. 6(c).
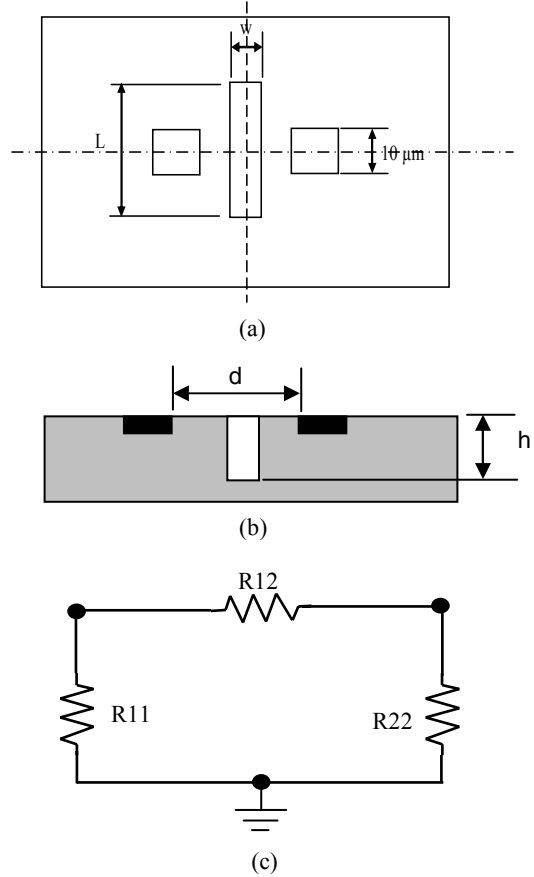

(a)

(b)

(c)

Fig. 6: Test configuration (not to scale). (a) The top view, (b) the cross section, and (c) the π-network.

First, let us assume the L-region is filled with silicon dioxide, i.e., the L-region is a trench. We consider both heavily and lightly doped substrates with typical cross sections shown in Fig. 7. Fig. 8 shows a comparison of R_{11}, R_{12} obtained from EPIC and ATLAS. There is a reasonably good agreement. For the heavily doped substrate, the relative errors of EPIC results with respect to the ATLAS are about 10% and 3% for R_{11} and R_{12}, respectively. For the lightly doped substrate, these errors are 6.0% and 8.5%, respectively. In both cases, the trench depth does not affect R_{11}. However, R_{12} shows a strong dependence on the trench depth, especially when the trench bottom is within the top layer of the

substrates (i.e., h < 1.0μm). R_{12} also depends on the trench length, as shown in Fig. 9, where R_{11} and R_{12} are shown as a function of the trench depth and length. An increase in the length of the trench increases R_{12}, especially when the trench depth is large. R_{11}, on the other hand, does not show a dependence on both the width and the length of the trench.
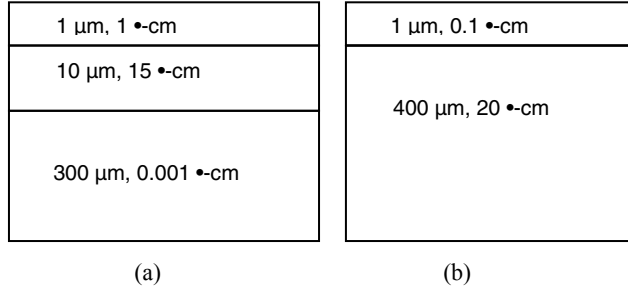
1 μm, 1 •-cm
10 μm, 15 •-cm
300 μm, 0.001 •-cm

(a)

1 μm, 0.1 •-cm
400 μm, 20 •-cm

(b)

Fig. 7: Resistivity and thickness of layered substrates. (a) A heavily doped substrate, and (b) a lightly doped substrate.

(a)

(b)
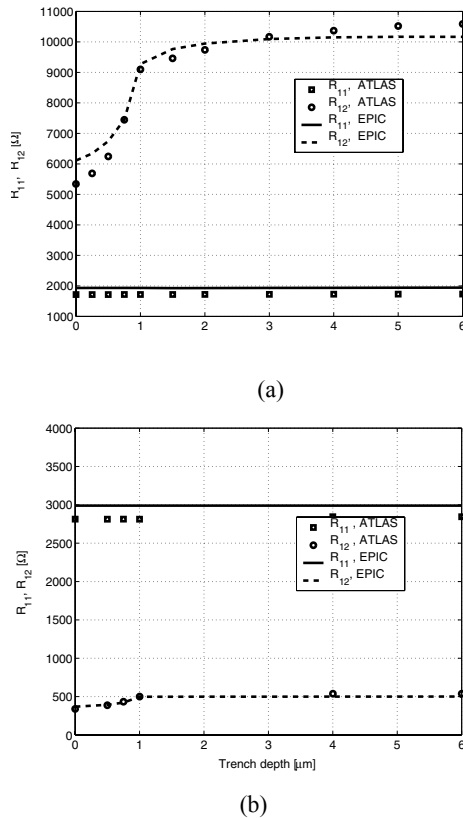
Fig. 8: Comparison of ATLAS and EPIC results for a trench. The separation between two identical square contacts is d = 8μm. The trench width (W) and length (L) are 2 μm and 10μm, respectively. (a) R_{11} and R_{12} as a function of the trench depth for the heavily doped substrate, and (b) R_{11} and R_{12} as a function of the trench depth for the lightly doped substrate.

Fig. 10 shows the computational time comparison between EPIC and ATLAS. The CPU cost in ATLAS mainly depends on the total number of grid nodes. For the simple example problem, the mesh was kept unchanged, and thus the CPU cost does not change with trench depth. The CPU cost of EPIC, however, increases as

the trench depth increases. There are two reasons for this increase. First, as the trench depth increases, more sets of DCT, DST and DSCT are needed. If the maximum number of panels in the z-direction is n, then $n(n-1)/2$ sets of DCT, DST and DSCT calculations are needed. Second, the increase in trench depth also increases the total number of virtual contacts, and the [P] matrix size in Eq. (1) increases.
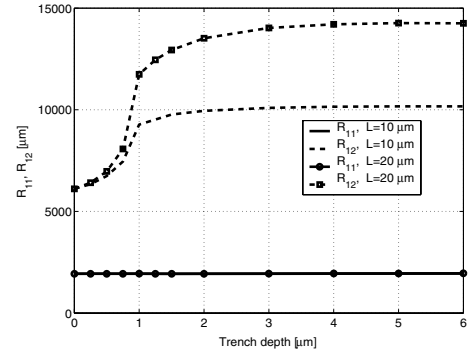

Fig. 9: Effect of the trench length (L) on R_{11} and R_{12} for the heavily doped substrate. The separation between the two identical square contacts is d = 8μm. The trench width (W) is 2.0 μm.
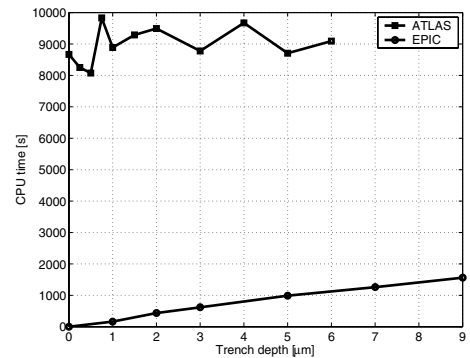

Fig. 10: CPU time as a function of trench depth.

To see the effect of the trench for different contact separations, the trench depth is fixed at 6 μm for a heavily doped substrate. Fig. 11 shows ratios of R_{11}/R_{11}^0 and R_{12}/R_{12}^0 as a function of contact separation, where R_{11}^0 and R_{12}^0 are the R_{11} and R_{12} values, respectively, when there is no trench between the two contacts. We see that, the ratio R_{11}/R_{11}^0 is a constant, indicating that R_{11} does not change much with separation. R_{12}/R_{12}^0, on the other hand, decreases as the separation increases, implying that for a given trench depth, there is less of an effect at large separations. In other words, if the separation between two contacts is large, increasing the trench depth may not be an effective way to improve the isolation (i.e., increase R_{12}) since the coupling current penetrates deeper into the heavily doped substrate.

To conclude this section, let's consider the effect of the L-region's resistivity on the resistance network, assuming the trench is filled with p-type silicon with different doping levels. Fig. 12 shows the coupling resistance as a function of the L-region's resistivity. The resistance value of 6112Ω is the R_{12} value without the L-region. As expected, a smaller resistivity results in a smaller R_{12}. The decrease in R_{11} is negligible. When the resistivity is less than that

of the substrate, then the L-region becomes a sinker, R_{12} becomes smaller than that in the case when there is no L-region. In other words, a sinker between two contacts increases the coupling between the contacts.
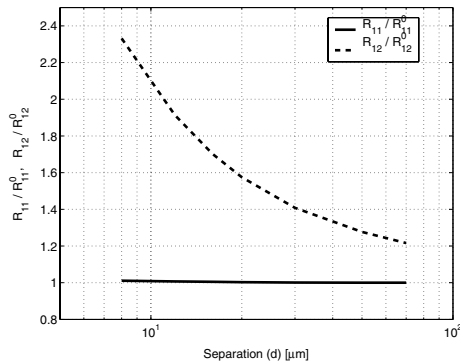

Fig. 11: Ratios of R_{11}/R_{11}^0 and R_{12}/R_{12}^0 as a function of separation in a heavily doped substrate.
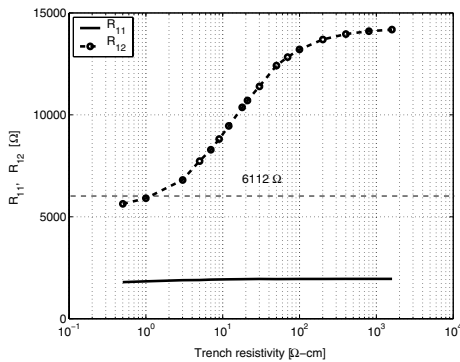

Fig. 12: Effect of L-region resistivity on R_{11}, and R_{12} for the heavily doped substrate. The contact separation is 8μm, and the trench length, width and depth are 20μm, 2μm and 6μm, respectively.

5. CONCLUSIONS

This paper presents a new approach to handle the parasitic extraction in substrates with inhomogeneous layers. Numerical simulations show that, the formulations are accurate, and, together with the use of DCT, DST, and MDSCT, the formulations are also computationally efficient. Compared with ATLAS this method has less than 10% error. Furthermore, the proposed approach can be several orders of magnitude faster than conventional device simulation or combined BEM/FDM/FEM approaches. respectively.

6. ACKNOWLEDGMENTS

7. REFERENCES

[1] B. R. Stanisic, N. K. Verghese, R. A. Rutenbar, R. L. Carley, and D. J. Allstot, "Addressing substrate coupling in mixed-mode IC's and power distribution synthesis," *IEEE J. Solid-State Circuits*, vol. 29, pp. 226-237, March 1994.

[2] P. Miliozzi, L. Carloni, E. Charbon, and A. Sangiovanni-Vincentelli, "SUBWAVE: a methodology for modeling digital substrate noise injection in mixed-signal ICs," *Proceedings of the IEEE Custom Integrated Circuits Conference,* pp. 385-388, May 1996.

[3] M. Pfost and H. M. Rein, "Modeling and measurement of substrate coupling in Si-Bipolar IC's up to 40 GHz," *IEEE J. Solid-State Circuits,* vol. 33, pp. 582-591, April 1998.

[4] S. Donnay and G. Gielen, *Substrate Noise Coupling in Mixed-signal ASICs*, Kluwer Academic Publishers, 2003.

[5] N. K. Verghese, T. Schmerbeck, and D.J. Allstot, *Simulation Techniques and Solutions for Mixed-Signal Coupling in ICs*, Kluwer Academic Publisher, 1995.

[6] X. Aragones, J. l. Gonzalez, and A. Rubio, *Analysis and Solutions for Switching Noise Coupling in Mixed-Signal ICs,* Kluwer Academic Publisher, 1999.

[7] E. Charbon, R. Gharpurey, P. Milliozzi, R.G. Meyer, and A. Sangiovanni-Vincentelli, *Substrate Noise: Analysis and Optimization for IC Design*, Kluwer Academic Publisher, 1995.

[8] T. A. Johnson, R. W. Knepper, V. Marcello, and W. Wang, "Chip substrate resistance modeling technique for integrated circuit design," *IEEE Trans. Computer-Aided Design*, vol. 3, pp. 126-134, April 1984.

[9] L. M. Silveira and N. Vargas, "Characterizing substrate coupling in deep-submicron designs," *IEEE Design & Test of Computers*, vol. 19, pp. 26-29, March-April 2002.

[10] R. Gharpurey, "Modeling and analysis of substrate coupling in IC's," *Ph.D. dissertation*, Univ. California, Berkeley, 1995.

[11] A. M. Niknejad, R. Gharpurey, and R. G. Meyer, "Numerically stable Green function for modeling and analysis of substrate coupling in integrated circuits," *IEEE Trans. Computer-Aided Design*, vol. 17, pp. 305-315, April 1998.

[12] J. P. Costa, M. Chou, and L. M. Silveira, "Efficient techniques for accurate modeling and simulation of substrate coupling in mixed-signal IC's," *IEEE Trans. Computer-Aided Design*, vol. 18, pp. 597-607, May 1999.

[13] H. Li, J. Carballido, H. H. Yu, V. I. Okhmatovski, E. Rosenbaum, and A. C. Cangellaris, "Comprehensive frequency-dependent substrate noise analysis using boundary element methods," *IEEE/ACM International Conference on Computer-Aided Design*, pp. 2-9, Nov. 2002.

[14] E. Schrik and N. R. van der Meijs, "Combined BEM/FEM substrate resistance modeling," *Proc. 39th Design Automation Conference*, pp. 771 − 776, June 2002.

[15] E. Schrik, P. M. Dewilde, and N. P. van der Meijs, "Theoretical and practical validation of combined BEM/FEM substrate resistance modeling," *IEEE/ACM International Conference on Computer Aided Design*, pp. 10-15, Nov. 2002.

[16] W. H. Press, B. P. Flannery, S. A. Teukolsky, and W. T. Vetterling, *Numerical Recipes in C*, Cambridge University Press, 1988.

[17] *ATLAS User's Manual*, SILVACO International.